

# Accepted Manuscript

Synthesis and in vitro biological evaluation of three 4'-(4-methoxyphenyl)-2,2':6',2''-terpyridine iridium(III) complexes as new telomerase inhibitors

Qi-Pin Qin, Ting Meng, Ming-Xiong Tan, Yan-Cheng Liu, Xu-Jian Luo, Bi-Qun Zou, Hong Liang



PII: S0223-5234(17)30827-9

DOI: [10.1016/j.ejmech.2017.10.035](https://doi.org/10.1016/j.ejmech.2017.10.035)

Reference: EJMECH 9827

To appear in: *European Journal of Medicinal Chemistry*

Received Date: 29 July 2017

Revised Date: 29 September 2017

Accepted Date: 12 October 2017

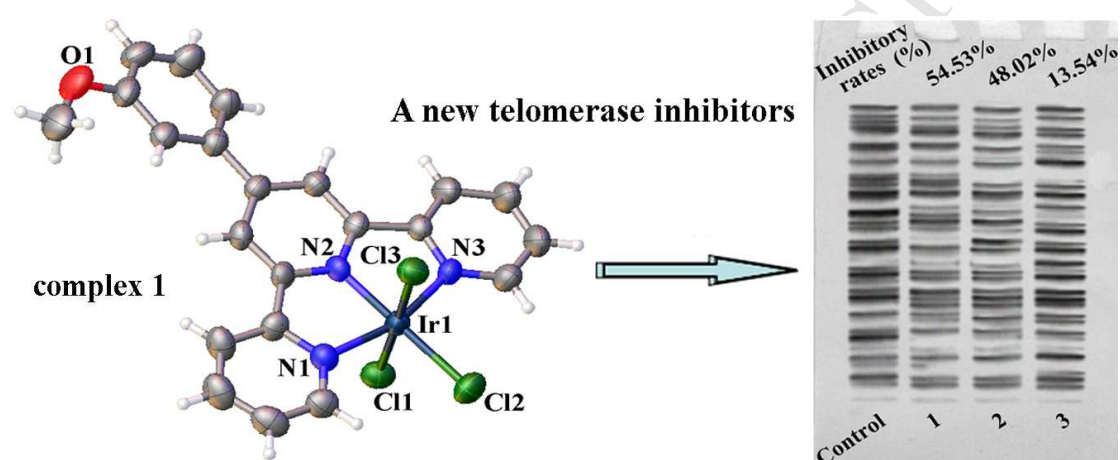
Please cite this article as: Q.-P. Qin, T. Meng, M.-X. Tan, Y.-C. Liu, X.-J. Luo, B.-Q. Zou, H. Liang, Synthesis and in vitro biological evaluation of three 4'-(4-methoxyphenyl)-2,2':6',2''-terpyridine iridium(III) complexes as new telomerase inhibitors, *European Journal of Medicinal Chemistry* (2017), doi: 10.1016/j.ejmech.2017.10.035.

This is a PDF file of an unedited manuscript that has been accepted for publication. As a service to our customers we are providing this early version of the manuscript. The manuscript will undergo copyediting, typesetting, and review of the resulting proof before it is published in its final form. Please note that during the production process errors may be discovered which could affect the content, and all legal disclaimers that apply to the journal pertain.

## Graphical abstract

Synthesis and *in vitro* biological evaluation of three  
 4'-(4-methoxyphenyl)-2,2':6',2''-terpyridine iridium(III)  
 complexes as new telomerase inhibitors

Qi-Pin Qin <sup>a,c,1</sup>, Ting Meng <sup>a,c,1</sup>, Ming-Xiong Tan <sup>a,c,\*</sup>, Yan-Cheng Liu <sup>c</sup>, Xu-Jian Luo <sup>a,c,\*</sup>, Bi-Qun Zou <sup>\*,b</sup>, Hong Liang <sup>c</sup>



1–3 directly targeted c-myc promoter elements and inhibited the telomerase activity. In addition, 1–3 may trigger cell apoptosis via a mitochondrial dysfunction pathway.

**Synthesis and *in vitro* biological evaluation of three  
4'-(4-methoxyphenyl)-2,2':6',2''-terpyridine iridium(III)  
complexes as new telomerase inhibitors**

Qi-Pin Qin <sup>a,c,1</sup>, Ting Meng <sup>a,c,1</sup>, Ming-Xiong Tan <sup>a,c,\*</sup>, Yan-Cheng Liu <sup>c</sup>, Xu-Jian Luo <sup>a,c,\*</sup>, Bi-Qun Zou <sup>\*,b</sup>, Hong Liang <sup>c</sup>

<sup>a</sup> Guangxi Key Laboratory of Agricultural Resources Chemistry and Biotechnology, College of Chemistry and Food Science, Yulin Normal University, 1303 Jiaoyudong Road, Yulin 537000, PR China.

<sup>b</sup> Department of Chemistry, Guilin Normal College, 15 Xinyi Road, Guilin 541001, PR China.

<sup>c</sup> State Key Laboratory for the Chemistry and Molecular Engineering of Medicinal Resources, School of Chemistry and Pharmacy, Guangxi Normal University, 15 Yucai Road, Guilin 541004, PR China.

\*Correspondence to:

E-mail: mxtan2018@126.com (M.-X. Tan), 2006315llxxjj@163.com (X.-J. Luo), zoubiqun@163.com (B.-Q. Zou)

Tel: +86-775-2623650

<sup>1</sup> These authors contributed equally to this work.

**Abstract**

Three iridium(III) complexes, [Ir(3-MeO-Phtpy)Cl<sub>3</sub>] (**1**), [Ir(2-MeO-Phtpy)Cl<sub>3</sub>] (**2**) and [Ir(4-MeO-Phtpy)Cl<sub>3</sub>] (**3**) with 4'-(3-methoxyphenyl)-2,2':6',2''-terpyridine (3-MeO-Phtpy), 4'-(2-methoxyphenyl)-2,2':6',2''-terpyridine (2-MeO-Phtpy) and 4'-(4-methoxyphenyl)-2,2':6',2''-terpyridine (4-MeO-Phtpy) as ligands, respectively, were synthesized and evaluated for their antiproliferative activities. In these complexes, the iridium(III) center adopts a six-coordinate distorted octahedral geometry. Among them, complex **1** exhibited the most potent activity, with IC<sub>50</sub> values of 3.19–27.77  $\mu$ M against four cancer cell lines (BEL-7404, Hep-G2, NCI-H460 and MGC80-3 cells). Cellular mechanism studies suggested that complexes **1–3** directly targeted c-myc promoter elements and inhibited the telomerase activity. In addition, complexes **1–3** may trigger cell apoptosis via a mitochondrial dysfunction pathway. We postulated that the difference in the *in vitro* antitumor activities of complexes **1–3** is mainly dependent on the position of the methoxy group on the phenyl ring of the iridium ligand.

**Keywords**

4'-substituted-2,2':6',2''-terpyridine, iridium(III) complexes, cell apoptosis, antitumor activity, telomerase activity

## 1. Introduction

Since G-quadruplex (G4) DNA is widely located in the chromosomal telomeric sequences as well as regulatory regions of oncogenes (such as KRAS, c-myc, HRAS, bcl-2, c-KIT and VEGF) [1–11], it is considered as an important regulator of a wide range of biological processes including translation, replication and splicing [1, 10–12]. The presence of G4 DNA in human cells has been firmly established using antibody [1, 10–13], thereby providing the basis for the elucidation of its functions in normal and disease states. Therefore, rational design of small molecule ligands to selectively interact and stabilize G4 DNA has been identified as a promising strategy for the development of anti-cancer drugs selective towards tumor cells against normal cells [1,14].

The c-myc oncoprotein is a transcription factor that plays essential roles in controlling cell proliferation, growth, and apoptosis as well as in regulating carcinogenic progression [1,10,11,14]. Deregulation of c-myc expression is associated with human tumors and cancers [1,10,11,14]. Thus, c-myc is an important drug target in oncology [1,10,11,14,15]. Strategies that aim to target c-myc both in the gene and protein levels, including those that interfere with c-myc synthesis, stability, and transcriptional activity, have emerged as effective anti-cancer therapies [1,10,11,14,15].

Recent studies have demonstrated that metal-terpyridine complexes with Zn(II), Cu(II), Pd(II), and Pt(II) ion centres can act as effective G4 ligands [16–26]. For example, Ang et al. designed four dinuclear Pt(II)-terpyridine complexes, which were shown as efficient G4 ligands [24]. A dinuclear Cu(II)-terpyridine complex was shown to effectively bind to G4 DNA and stabilize the antiparallel topology; its selectivity for G4 DNA is 100-fold higher than that for duplex DNA [1,25,26].

Bertrand et al. synthesized a range of Cu(II)-terpyridine complexes which displayed better affinity and selectivity for G4 DNA than similar complexes reported previously [1,16]. Nonetheless, little is known about the iridium(III) complexes with terpyridine and its derivatives as ligands and detailed studies on their molecular mechanisms of action are still lacking [27–31].

In this work, three iridium(III) complexes,  $[\text{Ir}(\text{3-MeO-Phtpy})\text{Cl}_3]$  (**1**),  $[\text{Ir}(\text{2-MeO-Phtpy})\text{Cl}_3]$  (**2**) and  $[\text{Ir}(\text{4-MeO-Phtpy})\text{Cl}_3]$  (**3**) with 4'-(3-methoxyphenyl)-2,2':6',2''-terpyridine (3-MeO-Phtpy), 4'-(2-methoxyphenyl)-2,2':6',2''-terpyridine (2-MeO-Phtpy) and 4'-(4-methoxyphenyl)-2,2':6',2''-terpyridine (4-MeO-Phtpy) as ligands, respectively, were synthesized and characterized by ESI-MS, IR spectroscopy, UV-vis spectroscopy, elemental analysis, single-crystal X-ray diffraction analysis, and NMR spectroscopy. In addition, the effects of these complexes on cell proliferation and apoptosis were evaluated.

## 2. Results and discussion

### 2.1 Synthesis and characterization

Synthesis of 4'-(3-methoxyphenyl)-2,2':6',2''-terpyridine (3-MeO-Phtpy), 4'-(2-methoxyphenyl)-2,2':6',2''-terpyridine (2-MeO-Phtpy) and 4'-(4-methoxyphenyl)-2,2':6',2''-terpyridine (4-MeO-Phtpy) was performed as described previously (Scheme 1) [27–33]. The three terpyridine ligands were individually incubated with  $\text{IrCl}_3$  in  $\text{CH}_3\text{OH}$  and  $\text{DMSO}$  (v:v= 25:1) at 80 °C for 48 h to obtain the corresponding iridium(III) metal complexes **1–3**. Their structures were characterized by spectroscopic and analytical methods, including ESI-MS, IR spectroscopy, UV-vis spectroscopy, elemental analysis, single-crystal X-ray

diffraction analysis, as well as NMR spectroscopy (Figs. S1–S18).

### [Scheme 1]

## 2.2 Crystal structures of complexes 1–3

The X-ray crystallographic data for complexes 1–3 are summarized in the Supporting Information (Tables S1–S9). In these complexes, the iridium(III) center is six-coordinate (three nitrogen ligands from the terpyridine moiety plus three chloride ligands) with a distorted octahedral geometry (Figs. 1–3). The Ir–N bond lengths are in the range of 1.948–2.043, 1.938–2.060 and 1.938–2.060 Å, respectively, which are within the normal range.

[Fig. 1]

[Fig. 2]

[Fig. 3]

## 2.3 Stability and solubility studies of complexes 1–3 in TBS and distilled water

The stability of complexes 1–3 ( $3.0 \times 10^{-5}$  M) in 10 mM Tris-HCl buffer solution (TBS), pH 7.35 was monitored by following the changes in the UV-vis, the conductivity experiment and ESI-MS spectra (Figs. S12, S15, S18–S20). The UV-vis spectra of the three complexes showed that they were stable in TBS for 48 h at room temperature. ESI-MS characterization of these complexes revealed the most abundant ions at  $m/z = 680.1$  for complexes 1 ( $[\text{Ir}^{\text{III}} + (3\text{-MeO-Phtpy}) + 2\text{Cl} + \text{DMSO}]^+$ ),  $m/z = 652.1$  for complexes 2 ( $[\text{Ir}^{\text{III}} + (2\text{-MeO-Phtpy}) + 3\text{Cl} + \text{H}_2\text{O} - \text{H}]^-$ ), and  $m/z = 680.1$  for complexes 3 ( $[\text{Ir}^{\text{III}} + (4\text{-MeO-Phtpy}) + 2\text{Cl} + \text{DMSO}]^+$ ). After 48-h incubation in TBS, there was no change in the  $m/z$  values of the most abundant ions, confirming that complexes 1–3 were stable under this condition. Moreover, the conductivity experiment was thus carried out for further assessment. As shown in Fig. S20, after the stock solution of complexes 1–3 and cisplatin at their  $\text{IC}_{50}$  concentrations were

diluted by cellular lysate (Hep-G2 cells) and was monitored immediately, the conductivity of cisplatin was observed to increase rapidly, comparing with three Ir(III) complexes **1–3** solution. Finally, the conductivity value of the cellular lysate (Hep-G2 cells) of complexes **1–3** and cisplatin boosted about 2.3, 2.4, 2.5 and 2.9 times in 48 h, respectively, therefore, it could be concluded that Ir(III) complexes **1–3** was more stable for 48 h in cellular lysate (Hep-G2 cells) than that of cisplatin, which further supported the stability analysis results of UV-Vis spectroscopy and ESI-MS. Taken together, three new Ir(III) complexes **1–3** during in the required time could retain a coordinated geometry with a positive charge under physiological conditions.

In addition, the solubility of three Ir(III) complexes **1–3** was investigated gravimetrically in distilled water by UV-vis spectroscopy [34], as shown in Fig. S21. The solubility of Ir(III) complexes **1–3** were over 0.16, 0.08 and 0.07 g/L in distilled water at room temperature, respectively.

#### **2.4 In vitro cytotoxicity**

To analyze the in vitro antitumor activity of 3-MeO-Phtpy, 2-MeO-Phtpy, 4-MeO-Phtpy, cisplatin, IrCl<sub>3</sub> and complexes **1–3**, we evaluated their cytotoxic effects on the BEL-7404, Hep-G2, NCI-H460 and MGC80-3 tumor cell lines using the normal human HL-7702 cells as a control. The MTT colorimetric assay was performed to estimate the IC<sub>50</sub> values of the compounds after a 48-h incubation of the cells with these compounds. As shown in Table 1 and S10, complexes **1–3** exhibited lower IC<sub>50</sub> values (IC<sub>50</sub>= 3.19–38.27 μM) against all the tested cancer cells than the corresponding IC<sub>50</sub> values of 3-MeO-Phtpy, 2-MeO-Phtpy, 4-MeO-Phtpy and IrCl<sub>3</sub>. Notably, in the Hep-G2 cells, complexes **1–3** showed higher cytotoxicity compared to cisplatin. Among these three complexes, complex **1** exhibited the highest cytotoxicity against all the tested cell lines, followed by complex **2** and then complex **3**. All three

complexes displayed higher cytotoxicity against the tumor cell lines compared to the normal HL-7702 cell line. As shown in Table 1, complex **1** exhibited a remarkably high selectivity index factor [36,37]. The high selectivity for the tumor cells rendered complex **1** to be a promising lead anti-tumor compound.

[Table 1]

### 2.5 Cellular uptake and distribution of complexes **1–3** in the Hep-G2 cells

Cellular uptake and distribution of complexes **1–3** in the Hep-G2 cells was measured using ICP-MS after a 24 h exposure to the complexes at their  $IC_{50}$  concentrations. As shown in Fig. 4A, the cellular uptake level of complex **1** was determined to be  $6.843 \pm 0.224$  nmol Ir /  $10^6$  cells, higher than the levels of complex **2** ( $5.027 \pm 0.107$  nmol Ir /  $10^6$  cells), complex **3** ( $3.945 \pm 0.209$  nmol Ir /  $10^6$  cells), and cisplatin ( $4.025 \pm 0.154$  nmol Pt /  $10^6$  cells). Thus, the high cytotoxicity of complex **1** might be caused by its high cellular uptake level. The cellular distribution of complexes **1–3** in the Hep-G2 cells was determined using the methods reported previously [38–41]. As shown in Fig. 4B, complexes **1–3** were accumulated in the nuclear fraction and the mitochondrial fraction, whereas cisplatin was mainly accumulated in the mitochondrial fraction. The cellular distribution of these compounds is likely related to the apoptotic pathways that they activated [38–41].

[Fig. 4]

### 2.6 Effects of complexes **1–3** on the expression of c-myc and hTERT in the Hep-G2 cells

Recent findings have unambiguously demonstrated that the expression level of hTERT is a key regulator of the telomerase activity [12,13]. The expression of hTERT is regulated by several factors. For example, c-myc is shown to induce the expression of hTERT, whereas the stimulating protein 1 (Sp1) suppresses it [42,43]. Herein, we

examined the effects of complexes **1–3** on the expression of c-myc and hTERT in the Hep-G2 cells. We found that treatment with complexes **1–3** for 24 h downregulated the expression of c-myc and hTERT genes and proteins in the Hep-G2 cells (Figs. 5 and 6). Notably, complex **1** displayed the most significant effect, followed by complex **2** and complex **3**.

[Fig. 5]

[Fig. 6]

### **2.7 Complexes 1–3 inhibited the telomerase activity**

Recent studies have demonstrated that the telomerase activity is elevated in immortalized cell lines, germinal cells, and in 85-90% of human cancer specimens, thereby supporting the role of telomerase in cell immortalization and in cancer/tumor progression [42,43]. To investigate the effects of complexes **1–3** on the telomerase activity in the Hep-G2 cells, the TRAP assay (TRAP-silver staining assay) was performed on the Hep-G2 cells treated with complexes **1–3**. As shown in Figs. 7 and S22, complexes **1–3** significantly inhibited the telomerase activity in the Hep-G2 cells. Again, complex **1** showed the highest inhibitory activity, followed by complex **2** and complex **3**.

[Fig. 7]

### **2.8 Transfection assay**

To probe whether complexes **1–3** directly regulated the c-myc promoter in the Hep-G2 cells, the cells were transfected by the enhanced green fluorescent protein (EGFP) plasmid or the c-myc plasmid (including c-myc G4 DNA promoter) was then examined by the luciferase reporter gene, using the methods reported previously [34,38,40,44,45]. Compared with the untreated group, the Hep-G2 cells with the EGFP plasmid transfection emitted green fluorescence (Fig. 8A), indicating that the

transfection was successful. In the Hep-G2 cells transfected with the c-myc plasmid, treatment with complexes **1–3** on the Hep-G2 cells induced a pronounced decrease of the fluorescence signal in the luciferase assay, suggesting that complexes **1–3** directly targeted the c-myc promoter (Fig. 8B). Complex **1** caused the most significant decrease of the fluorescence signal (from 100.0% to ca. 20.3%).

[Fig. 8]

### **2.9 Mitochondrial membrane potential ( $\Delta\psi$ )**

Mitochondria plays a crucial role in the induction and control of apoptosis through the release of proapoptotic factors such as cytochrome c (cyt c) [46,47]. As shown in Fig. 4, complexes **1–3** were accumulated in the mitochondrial fraction and the nuclear fraction. Therefore, alterations in the mitochondrial membrane potential ( $\Delta\psi$ ) were measured in the Hep-G2 cells using an inverted fluorescence microscope after staining the cells with the JC-1 cationic dye (Fig. 9). JC-1 can aggregate on intact mitochondria with normal  $\Delta\psi$  values and form red fluorescence as a result of the aggregation. When the mitochondria membrane is depolarized and an abnormal  $\Delta\psi$  is present, JC-1 remains as monomers and emits green fluorescence. Treatment with complexes **1–3** at their  $IC_{50}$  concentrations caused a decrease in the intensity of the red fluorescence signal and an increase in the intensity of the green fluorescence signal. This result indicates the cytotoxicity of complexes **1–3** is associated with a mitochondrial pathway [46,47].

[Fig. 9]

### **2.10 Effects of complexes 1-3 on intracellular ROS generation**

Many anticancer agents have been shown to induce the generation of reactive oxygen species (ROS) [48,49], which are considered as key mediators of apoptotic signaling. We investigated the effects of complexes **1–3** in inducing the production of ROS in

the Hep-G2 cells. The production of ROS was examined by using an oxidant-sensitive fluorescent probe, 2',7'-dichlorofluoresceindiacetate (DCFDA). After treatment with complexes **1–3** at their IC<sub>50</sub> concentrations for 24 h, the level of ROS in the Hep-G2 cells was significantly increased, as shown in Fig. 10. The results demonstrated that complexes **1–3** induced the generation of ROS. Among these three complexes, complex **1** induced the highest level of ROS.

[Fig. 10]

### **2.11 Effects of complexes 1–3 on the expression of apoptosis related proteins in the Hep-G2 cells**

To further elucidate the molecular mechanisms involved in the cytotoxicity of complexes **1–3**, we investigated the effects of these three complexes on the expression of proteins important for mitochondria-mediated apoptosis. As shown in Fig. 11, we found that complexes **1–3** were able to decrease the expression level of bcl-2 in the Hep-G2 cells. In contrast, the expression of p53, bax, cyt c, and apaf-1 was increased after the treatment with complexes **1–3**. These proteins are involved in the induction of mitochondrial membrane depolarization and cell apoptosis [48–50]. Accordingly, a recent study has demonstrated that DNA damage in mitochondria possibly through increased ROS generation and activation of a DNA damage response [51–58]. Moreover, 53BP1 plays a potential role in DNA damage responses and binds to the tumor suppressor protein p53 [39,59]. Thus, to verify the effects of Ir(III) complexes **1–3** on mitochondrial fraction in Hep-G2 cells, we carried out Western blot analyses on 53BP1 protein in Hep-G2 cells and showed the results in Fig. 23. Compared with the control group cells, significant increases of 53BP1 level on mitochondrial fraction in Hep-G2 cells were observed, suggesting that Ir(III) complexes **1–3** significantly induced DNA damages on mitochondrial fraction in BEL-7404 cells [51–59].

[Fig. 11]

### 2.12 Activation of caspase-3 and caspase-9

The activation of caspase-3 and caspase-9 plays an important role in the process of programmed cell death and apoptosis [49,60]. We monitored the activation of caspase-3 and caspase-9 in the Hep-G2 cells upon the treatment with complexes 1–3 for 24 h. Compared to the untreated cells, the treated cells showed activation of caspase-3 and caspase-9 (Fig. 12), suggesting that complexes 1–3 induced cell death via apoptosis in the Hep-G2 cells [49,60]. The cells treated with complex 1 showed the highest levels of activated caspase-3 and caspase-9.

[Fig. 12]

### 2.13 Cell apoptosis

As demonstrated in the sections above, complexes 1–3 directly regulated c-myc promoter, inhibited the expression of c-myc and hTERT, disrupted the mitochondrial function, and ultimately led to cell apoptosis [34,38,40,48–50,60–62]. The apoptotic effects of complexes 1–3 were evaluated by the Annexin V FITC and PI dual staining assay, which can examine the occurrence of phosphatidylserine externalization and determine whether this is caused by physiological apoptosis or nonspecific necrosis [34,38,40,48–50,60–62]. The Hep-G2 cells were treated with complexes 1–3 at their IC<sub>50</sub> concentrations for 24 h. As shown in Fig. 13, the result of the staining assay confirmed that the treatment with the complexes caused apoptosis in the Hep-G2 cells. Complex 1 induced the highest level of cell apoptosis, followed by complex 2 and complex 3.

[Fig. 13]

## 3. Conclusion

In this study, three iridium(III) complexes with terpyridine ligands were synthesized and characterized by different spectroscopic and analytic techniques. These complexes exhibited higher cytotoxicity against different cell lines compared to the terpyridine ligands. More importantly, they showed selective cytotoxicity against the tumor cell lines. In vitro assays with the Hep-G2 tumor cells revealed that complexes **1–3** acted as a telomerase inhibitor by directly targeting the c-myc promoter elements. Moreover, complexes **1–3** triggered the Hep-G2 cell apoptosis via a mitochondrial dysfunction pathway, which caused ROS generation, disruption of  $\Delta\psi$ , downregulation of the expression of bcl-2 and upregulation the expression of p53, bax, cyt c, 53BP1 and apaf-1. It should be noted that complex **1** showed the highest cytotoxicity among the three complexes. The high cytotoxicity of complex **1** was postulated to be related to the substitution position of the methoxy group on the terpyridine moiety. The 3-MeO substitution corresponded to highest level of cellular uptake. Taken together, complex **1** is an excellent lead compound for the development of new telomerase inhibitors.

## **4. Experimental methods**

### **4.1 Synthesis**

#### **4.1.1 Synthesis and characterization of the terpyridine ligands**

Synthesis of 4'-(3-methoxyphenyl)-2,2':6',2''-terpyridine (3-MeO-Phtpy), 4'-(2-methoxyphenyl)-2,2':6',2''-terpyridine (2-MeO-Phtpy) and 4'-(4-methoxyphenyl)-2,2':6',2''-terpyridine (4-MeO-Phtpy) were performed using the methods described previously [27–33]. 2-Acetylpyridine (2.813 g, 23.2 mmol, 2 eq.) was added to 2-methoxybenzaldehyde, 3-methoxybenzaldehyde or 4-methoxybenzaldehyde (11.6 mmol, 1 eq.) dissolved in 50 mL ethanol. KOH pellets

(46.5 mmol, 4 eq.) were added to this solution. The reaction mixture was stirred at room temperature for 10 min.  $\text{NH}_3$  (40 mL, 25% aq.) was slowly added to the reaction mixture. After a 24-h incubation at 34 °C, 5 mL of 25% aq.  $\text{NH}_3$  was added to the reaction mixture again. The flask containing the reaction mixture was cooled to -20 °C. The obtained white precipitate in the flask was isolated through filtration and washed with cold ethanol. We further purified the each product using recrystallization in ethanol- $\text{H}_2\text{O}$ . After recrystallization, each product was recovered by filtration, washed with cold ethanol and petroleum ether, and dried under high vacuum for 24 h (Scheme 1).

Characterization of 3-MeO-Phtpy. Yield: 45.62%. ESI-MS:  $m/z = 701.4$  for  $[2\text{M}+\text{Na}]^+$ ,  $m/z = 362.1$  for  $[\text{M}+\text{Na}]^+$ .  $^1\text{H}$  NMR (600 MHz,  $\text{DMSO-}d_6$ ):  $\delta$  8.68 (s, 2H), 8.55 (d,  $J = 7.6$  Hz, 4H), 7.94 (s, 2H), 7.44 (s, 2H), 7.41 (s, 1H), 7.34 (s, 1H), 7.28 (s, 1H), 7.03 (s, 1H), 3.80 (s, 3H). Elemental analysis: calcd (%) for  $\text{C}_{22}\text{H}_{17}\text{N}_3\text{O}$ : C 77.86, H 5.05, N 12.38; found: C 77.81, H 5.10, N 12.35.

Characterization of 2-MeO-Phtpy. Yield: 45.62%. ESI-MS:  $m/z = 701.4$  for  $[2\text{M}+\text{Na}]^+$ ,  $m/z = 362.1$  for  $[\text{M}+\text{Na}]^+$ .  $^1\text{H}$  NMR (600 MHz,  $\text{DMSO-}d_6$ ):  $\delta$  8.71 (s, 2H), 8.56 (s, 2H), 8.00 (s, 2H), 7.86 (d,  $J = 8.1$  Hz, 2H), 7.78 (s, 2H), 7.25 (s, 1H), 7.11 (s, 1H), 6.99 (s, 1H), 6.91 (s, 1H), 3.81 (s, 3H). Elemental analysis: calcd (%) for  $\text{C}_{22}\text{H}_{17}\text{N}_3\text{O}$ : C 77.86, H 5.05, N 12.38; found: C 77.84, H 5.08, N 12.34.

Characterization of 4-MeO-Phtpy. Yield: 45.62%. ESI-MS:  $m/z = 701.4$  for  $[2\text{M}+\text{Na}]^+$ ,  $m/z = 362.1$  for  $[\text{M}+\text{Na}]^+$ .  $^1\text{H}$  NMR (600 MHz,  $\text{DMSO-}d_6$ ):  $\delta$  8.77 (s, 2H), 8.66 (s, 4H), 7.96 (d,  $J = 93.6$  Hz, 4H), 7.53 (s, 2H), 7.13 (s, 2H), 3.86 (s, 3H). Elemental analysis: calcd (%) for  $\text{C}_{22}\text{H}_{17}\text{N}_3\text{O}$ : C 77.86, H 5.05, N 12.38; found: C 77.89, H 5.07, N 12.33.

#### 4.1.2 Synthesis and characterization of complexes 1–3

$\text{IrCl}_3$  (0.0299 g, 0.1 mmol) was mixed with 3-MeO-Phtpy, 2-MeO-Phtpy or 4-MeO-Phtpy (0.0339 g, 0.1 mmol), 0.20 mL DMSO and 0.50 mL  $\text{CH}_3\text{OH}$  in a Pyrex tube. The Pyrex tube containing the reaction mixture was then placed in liquid  $\text{N}_2$ , vacuumed and sealed. The reaction was initiated by heating the reaction mixture to 80 °C. After two days of incubation at 80 °C, the resulting brown-black crystals were isolated and characterized by different spectroscopic and analytic techniques

Characterization of complex **1**. Yield: 92.20%.  $^1\text{H}$  NMR (600 MHz,  $\text{DMSO-}d_6$ ):  $\delta$  8.87 (s, 4H), 8.75 (s, 2H), 8.32 (s, 2H), 7.78 (s, 2H), 7.52 (s, 2H), 7.47 (s, 1H), 7.10 (s, 1H), 3.87 (s, 3H). ESI-MS:  $m/z = 680.1$  for  $[\text{M}-\text{Cl}+\text{DMSO}]^+$ . IR (KBr): 3913, 3887, 3782, 3697, 3658, 3432, 3065, 2942, 2839, 1603, 1547, 1473, 1406, 1352, 1265, 1214, 1164, 1100, 1028, 904, 849, 787, 731, 688, 651, 517, 461  $\text{cm}^{-1}$ . Elemental analysis: calcd (%) for  $\text{C}_{22}\text{H}_{17}\text{Cl}_3\text{IrN}_3\text{O}$ : C 41.42, H 2.69, N 6.59; found: C 41.39, H 2.65, N 6.60.

Characterization of complex **2**. Yield: 85.30%.  $^1\text{H}$  NMR (600 MHz,  $\text{DMSO-}d_6$ ):  $\delta$  8.87 (d,  $J = 6.9$  Hz, 4H), 8.66 (s, 2H), 8.33 (s, 2H), 7.78 (s, 2H), 7.58 (s, 1H), 7.50 (s, 1H), 7.22 (s, 1H), 7.15 (s, 1H), 3.84 (s, 3H). ESI-MS:  $m/z = 652.1$  for  $[\text{M}+\text{H}_2\text{O}-\text{H}]^-$ . IR (KBr): 3913, 3887, 3783, 3695, 3658, 3432, 3069, 2973, 2842, 1601, 1542, 1496, 1469, 1410, 1295, 1247, 1161, 1130, 1098, 1051, 1014, 889, 843, 791, 760, 655, 636  $\text{cm}^{-1}$ . Elemental analysis: calcd (%) for  $\text{C}_{22}\text{H}_{17}\text{Cl}_3\text{IrN}_3\text{O}$ : C 41.42, H 2.69, N 6.59; found: C 41.35, H 2.73, N 6.57.

Characterization of complex **3**. Yield: 80.90%.  $^1\text{H}$  NMR (600 MHz,  $\text{DMSO-}d_6$ ):  $\delta$  8.89 (d,  $J = 7.8$  Hz, 2H), 8.86 (s, 2H), 8.73 (s, 2H), 8.34 (s, 2H), 7.95 (s, 2H), 7.79 (s, 2H), 7.11 (s, 2H), 3.83 (s, 3H). ESI-MS:  $m/z = 680.1$  for  $[\text{M}-\text{Cl}+\text{DMSO}]^+$ . IR (KBr): 3957, 3913, 3783, 3696, 3659, 3633, 3574, 3459, 3067, 2957, 2836, 1560, 1519, 1464, 1435, 1409, 1304, 1241, 1189, 1121, 1026, 889, 829, 790, 759, 726, 653, 601, 519,

461, 430  $\text{cm}^{-1}$ . Elemental analysis: calcd (%) for  $\text{C}_{22}\text{H}_{17}\text{Cl}_3\text{IrN}_3\text{O}$ : C 41.42, H 2.69, N 6.59; found: C 41.37, H 2.71, N 6.56.

#### 4.2 Instrumentation, materials and other experimental methods

The instrumentation, materials, and methods of different in vitro assays and experiments, including the MTT assay, determination of the cellular uptake and distribution of complexes **1–3**, the JC-1 staining assay, detection of ROS generation, cell apoptosis analysis, western blot, RT-PCR, and the transfection assay, were described in Ng and Chen previously published work [34,37–40,63]. The TRAP-silver staining assay was performed using methods reported previously [62,64].

#### Supporting Information

Vendor codes for 3-MeO-Phtpy, 2-MeO-Phtpy, 4-MeO-Phtpy and complexes **1–3**, inhibitory rates (%) against the selected five human cell lines, as well as ESI-MS, UV-vis,  $^1\text{H}$  NMR, IR and crystallographic data. In addition, CCDC No. 1561943, 1561944 and 1561950 for iridium(III) complexes **1–3** contains the supplementary crystallographic data for this paper.

#### Acknowledgement

This work was supported by the National Natural Science Foundation of China (No. 21261025, 21761033), the Key Foundation Project of Colleges and Universities in Guangxi (No. ZD2014108), the Innovative Team & Outstanding Talent Program of Colleges and Universities in Guangxi (2014-49), IRT\_16R15, the project of guibei characteristic medicine resources research center of Guangxi Province (KYA201703), the basic skills improvement project for the young and middle-aged teachers in Guangxi colleges and universities (KY2016YB595) as well as the State Key

Laboratory for the Chemistry and Molecular Engineering of Medicinal Resources,  
Ministry of Science and Technology of China (CMEMR2017-B17).

## References

## References

- [1] Q. Cao, Y. Li, E. Freisinger, P. Z. Qin, R.K.O. Sigel, Z.-W. Mao, G-quadruplex DNA targeted metal complexes acting as potential anticancer drugs, *Inorg. Chem. Front.* 4 (2017) 10–32.
- [2] T.-M. Ou, Y.-J. Lu, J.-H. Tan, Z.-S. Huang, K.-Y. Wong, L.-Q. Gu, G-quadruplexes: targets in anticancer drug design, *ChemMedChem* 3 (2008) 690–713.
- [3] A. Siddiqui-Jain, C.L. Grand, D.J. Bearss, L.H. Hurley, Direct evidence for a G-quadruplex in a promoter region and its targeting with a small molecule to repress c-MYC transcription, *Proc. Natl. Acad. Sci. U.S.A.* 99 (2002) 11593–11598.
- [4] S. Cogoi, L.E. Xodo, G-quadruplex formation within the promoter of the KRAS proto-oncogene and its effect on transcription, *Nucleic Acids Res.* 34 (2006) 2536–2549.
- [5] A. Membrino, S. Cogoi, E.B. Pedersen, L.E. Xodo, G4-DNA formation in the HRAS promoter and rational design of decoy oligonucleotides for cancer therapy, *PloS one* 6 (2011) e24421.
- [6] S. Rankin, A.P. Reszka, J. Huppert, M. Zloh, G.N. Parkinson, A.K. Todd, S. Ladame, S. Balasubramanian, S. Neidle, Putative DNA quadruplex formation within the human c-kit oncogene, *J. Am. Chem. Soc.* 127 (2005) 10584–10589.
- [7] D. Sun, W.-J. Liu, K. Guo, J.J. Rusche, S. Ebbinghaus, V. Gokhale, L.H. Hurley, The proximal promoter region of the human vascular endothelial growth factor gene has a G-quadruplex structure that can be targeted by G-quadruplex-interactive agents,

Mol. Cancer Ther. 7 (2008) 880–889.

[8] D. Sun, K. Guo, Y.J. Shin, Evidence of the formation of G-quadruplex structures in the promoter region of the human vascular endothelial growth factor gene, *Nucleic Acids Res.* 39 (2010) 1256–1265.

[9] S. Cogoi, A.E. Shchekotikhin, A. Membrino, Y.B. Sinkevich, L.E. Xodo, Guanidino anthrathiophenediones as G-quadruplex binders: uptake, intracellular localization, and anti-Harvey-Ras gene activity in bladder cancer cells, *J. Med. Chem.* 56 (2013) 2764–2778.

[10] Y. Jiang, A.-C. Chen, G.-T. Kuang, S.-K. Wang, T.-M. Ou, J.-H. Tan, D. Li, Z.-S. Huang, Design, synthesis and biological evaluation of 4-anilinoquinazoline derivatives as new c-myc G-quadruplex ligands, *Eur. J. Med. Chem.* 122 (2016) 264–279.

[11] H.-Y. Liu, A.-C. Chen, Q.-K. Yin, Z. Li, S.-M. Huang, G. Du, J.-H. He, L.-P. Zan, S.-K. Wang, Y.-H. Xu, J.-H. Tan, T.-M. Ou, D. Li, L.-Q. Gu, Z.-S. Huang, New disubstituted quindoline derivatives inhibiting Burkitt's lymphoma cell proliferation by impeding c-MYC transcription, *J. Med. Chem.* 60 (2017) 5438–5454.

[12] D. Rhodes, H.J. Lipps, G-quadruplexes and their regulatory roles in biology, *Nucleic Acids Res.* 43 (2015) 8627–8637.

[13] G. Biffi, D. Tannahill, J. McCafferty, S. Balasubramanian, Quantitative visualization of DNA G-quadruplex structures in human cells, *Nat. Chem.* 5 (2013) 182–186.

[14] S. Pelengaris, M. Khan, G.I. Evan, Suppression of Myc-induced apoptosis in  $\beta$  cells exposes multiple oncogenic properties of Myc and triggers carcinogenic progression, *Cell* 109 (2002) 321–334.

[15] L. Soucek, J. Whitfield, C.P. Martins, A.J. Finch, D.J. Murphy, N.M. Sodikin, A.N.

Karnezis, L.B. Swigart, S. Nasi, G.I. Evan, Modelling Myc inhibition as a cancer therapy, *Nature* 455 (2008) 679–683.

[16] H. Bertrand, D. Monchaud, A. De Cian, R. Guillot, J.-L. Mergny, M.-P. Teulade-Fichou, The importance of metal geometry in the recognition of G-quadruplex-DNA by metal-terpyridine complexes, *Org. Biomol. Chem.* 5 (2007) 2555–2559.

[17] P. Wang, C.-H. Leung, D.-L. Ma, S.-C. Yan, C.-M. Che, Structure-based design of platinum(II) complexes as c-myc oncogene down-regulators and luminescent probes for G-quadruplex DNA, *Chem. Eur. J.* 16 (2010) 6900–6911.

[18] S. Gama, I. Rodrigues, F. Mendes, I.C. Santos, E. Gabano, B. Klejevskaja, J. Gonzalez-Garcia, M. Ravera, R. Vilar, A. Paulo, Anthracene-terpyridine metal complexes as new G-quadruplex DNA binders, *J. Inorg. Biochem.* 160 (2016) 275–286.

[19] C. Wei, L. Ren, N. Gao, Interactions of terpyridines and their Pt(II) complexes with G-quadruplex DNAs and telomerase inhibition, *Int. J. Biol. Macromol.* 57 (2013) 1–8.

[20] E. Largy, F. Hamon, F. Rosu, V. Gabelica, E. De Pauw, A. Guédin, J.-L. Mergny, M.-P. Teulade-Fichou, Tridentate N-donor palladium(II) complexes as efficient coordinating quadruplex DNA binders, *Chem. Eur. J.* 17 (2011) 13274–13283.

[21] K. Suntharalingam, A.J.P. White, R. Vilar, Synthesis, structural characterization, and quadruplex DNA binding studies of platinum(II)-terpyridine complexes, *Inorg. Chem.* 48 (2009) 9427–9435.

[22] J.-T. Wang, Y. Li, J.-H. Tan, L.-N. Ji, Z.-W. Mao, Platinum(II)-triarylpyridines complexes with electropositive pendants as efficient G-quadruplex binders, *Dalton Trans.* 40 (2011) 564–566.

- [23] C. Yu, K.H.Y. Chan, K.M.-C. Wong, V. W.-W. Yam, Nucleic acid-induced self-assembly of a platinum(II) terpyridyl complex: detection of G-quadruplex formation and nuclease activity, *Chem. Commun.* (2009) 3756–3758.
- [24] D.L. Ang, B.W. J. Harper, L. Cubo, O. Mendoza, R. Vilar, J. Aldrich-Wright, Quadruplex DNA-stabilising dinuclear platinum(II) terpyridine complexes with flexible linkers, *Chem. Eur. J.* 22 (2016) 2317–2325.
- [25] K. Suntharalingam, A.J.P. White, R. Vilar, Two metals are better than one: investigations on the interactions between dinuclear metal complexes and quadruplex DNA, *Inorg. Chem.* 49 (2010) 8371–8380.
- [26] V.S. Stafford, K. Suntharalingam, A. Shivalingam, A.J.P. White, D.J. Mann, R. Vilar, Syntheses of polypyridyl metal complexes and studies of their interaction with quadruplex DNA, *Dalton Trans.* 44 (2015) 3686–3700.
- [27] A. Jacques, A. Kirsch-De Mesmaeker, B. Elias, Selective DNA purine base photooxidation by bis-terdentate iridium(III) polypyridyl and cyclometalated complexes, *Inorg. Chem.* 53 (2014) 1507–1512.
- [28] B.N. Mongal, S. Naskar, Synthesis, characterization, electrochemical and theoretical study of substituted phenyl-terpyridine and pyridine-quinoline based mixed chelate ruthenium complexes, *J. Coord. Chem.* 70 (2017) 451–462.
- [29] W. Leslie, A.S. Batsanov, J.A.K. Howard, J.A.G. Williams, Cross-couplings in the elaboration of luminescent bis-terpyridyl iridium complexes: the effect of extended or inhibited conjugation on emission, *Dalton Trans.* (2004) 623–631.
- [30] M. Cavazzini, P. Pastorelli, S. Quici, F. Loiseau, S. Campagna, Two-color luminescence from a tetranuclear Ir(III)/Ru(II) complex, *Chem. Commun.* (2005) 5266–5268.
- [31] L.S. Natrajan, A. Toulmin, A. Chew, S.W. Magennis, Two-photon

luminescence from polar bis-terpyridyl-stilbene derivatives of Ir(III) and Ru(II), Dalton Trans. 39 (2010) 10837–10846.

[32] J. Wang, G.S. Hanan, A facile route to sterically hindered and non-hindered 4'-aryl-2, 2': 6', 2''-terpyridines, Synlett 2005 (2005) 1251–1254.

[33] Y. Li, M. Cheng, J. Hao, C. Wang, G. Jia, C. Li, Terpyridine-Cu(II) targeting human telomeric DNA to produce highly stereospecific G-quadruplex DNA metalloenzyme, Chem. Sci. 6 (2015) 5578–5585.

[34] Z.-F. Chen, Q.-P. Qin, J.-L. Qin, Y.-C. Liu, K.-B. Huang, Y.-L. Li, T. Meng, G.-H. Zhang, Y. Peng, X.-J. Luo, H. Liang, Stabilization of G-quadruplex DNA, inhibition of telomerase activity and tumor cell apoptosis of organoplatinum(II) complexes with oxoisoaporphine, J. Med. Chem. 58 (2015) 2159–2179.

[35] R. Cao, J.-L. Jia, X.-C. Ma, M. Zhou, H. Fei, Membrane localized iridium(III) complex induces endoplasmic reticulum stress and mitochondria-mediated apoptosis in human cancer cells, J. Med. Chem. 56 (2013) 3636–3644.

[36] H.-Y. Zhou, F.-Q. Dong, X.-L. Du, Z.-K. Zhou, H.-R. Huo, W.-H. Wang, H.-D. Zhan, Y.-F. Dai, J. Meng, Y.-P. Sui, J. Li, F. Sui, Y.-H. Zhai, Antitumor activities of biscoumarin and dihydropyran derivatives, Bioorg. Med. Chem. Lett. 26 (2016) 3876–3880.

[37] Q.-P. Qin, T. Meng, Z.-Z. Wei, C.-H. Zhang, Y.-C. Liu, H. Liang, Z.-F. Chen, Synthesis, crystal structure, cytotoxicity, and mechanism of action of Zn<sup>II</sup>, Mn<sup>II</sup>, and Fe<sup>III</sup> complexes with 6-hydroxyoxoisoaporphine, Eur. J. Inorg. Chem. 2017 (2017) 1824–1834.

[38] J.-L. Qin, Q.-P. Qin, Z.-Z. Wei, C.-C. Yu, T. Meng, C.-X. Wu, Y.-L. Liang, H. Liang, Z.-F. Chen, Stabilization of c-myc G-quadruplex DNA, inhibition of telomerase activity, disruption of mitochondrial functions and tumor cell apoptosis by

platinum(II) complex with 9-amino-oxoisoaporphine, *Eur. J. Med. Chem.* 124 (2016) 417–427.

[39] Z.-F. Chen, Q.-P. Qin, J.-L. Qin, J. Zhou, Y.-L. Li, N. Li, Y.-C. Liu, H. Liang, Water-soluble ruthenium(II) complexes with chiral 4-(2,3-dihydroxypropyl)-formamide oxoaporphine (FOA): In vitro and in vivo anticancer activity by stabilization of G-Quadruplex DNA, inhibition of telomerase activity, and induction of tumor cell apoptosis, *J. Med. Chem.* 58 (2015) 4771–4789.

[40] Q.-P. Qin, J.-L. Qin, T. Meng, W.-H. Lin, C.-H. Zhang, Z.-Z. Wei, J.-N. Chen, Y.-C. Liu, H. Liang, Z.-F. Chen, High in vivo antitumor activity of cobalt oxoisoaporphine complexes by targeting G-quadruplex DNA, telomerase and disrupting mitochondrial functions, *Eur. J. Med. Chem.* 124 (2016) 380–392.

[41] E. Schreiber, P. Matthias, M.M. Mueller, W. Schaffner, Rapid detection of octamer binding proteins with ‘mini-extracts’ prepared from a small number of cells, *Nucleic Acids Res.* 17 (1989) 6419.

[42] J.C. Poole, L.G. Andrews, T.O. Tollefsbol, Activity, function, and gene regulation of the catalytic subunit of telomerase (hTERT), *Gene* 269 (2001) 1–12.

[43] H.-S. Huang, J.-F. Chiou, Y. Fong, C.-C. Hou, Y.-C. Lu, J.-Y. Wang, J.-W. Shih, Y.-R. Pan, J.-J. Lin, Activation of human telomerase reverse transcriptase expression by some new symmetrical bis-substituted derivatives of the anthraquinone, *J. Med. Chem.* 46 (2003) 3300–3307.

[44] M. Chalfie, Y. Tu, G. Euskirchen, W.W. Ward, D.C. Prasher, Green fluorescent protein as a marker for gene expression, *Science* 263 (1994) 802–805.

[45] T.-C. He, A.B. Sparks, C. Rago, H. Hermeking, L. Zawel, L.T. da Costa, P.J. Morin, B. Vogelstein, K.W. Kinzler, Identification of c-MYC as a target of the APC pathway, *Science* 281 (1998) 1509–1512.

- [46] A. Elkamhawy, J.-E. Park, A.H.E. Hassand, H. Ra, A.N. Pae, J. Lee, B.-G. Park, B. Moon, H.-M. Park, E.J. Roh, Discovery of 1-(3-(benzyloxy)pyridin-2-yl)-3-(2-(piperazin-1-yl) ethyl) urea: A new modulator for amyloid beta-induced mitochondrial dysfunction, *Eur. J. Med. Chem.* 128 (2017) 56–69.
- [47] P. Sakthivel, A. Ilangoan, M.P. Kaushik, Natural product-inspired rational design, synthesis and biological evaluation of 2, 3-dihydropyrano [2, 3-f] chromen-4 (8H)-one based hybrids as potential mitochondrial apoptosis inducers, *Eur. J. Med. Chem.* 122 (2016) 302–318.
- [48] V. Vichai, K. Kirtikara, Sulforhodamine B colorimetric assay for cytotoxicity screening, *Nat. Protoc.* 1 (2006) 1112–1116.
- [49] D. Yugandhar, V.L. Nayak, S. Archana, K.C. Shekar, A.K. Srivastav, Design, synthesis and anticancer properties of novel oxa/azaspiro [4, 5] trienones as potent apoptosis inducers through mitochondrial disruption, *Eur. J. Med. Chem.* 101 (2015) 348–357.
- [50] S. Li, S. Zhang, X. Jin, X. Tan, J. Luo, X. Zhang, Y. Zhao, Singly protonated dehydronorcantharidin silver coordination polymer induces apoptosis of lung cancer cells via reactive oxygen species-mediated mitochondrial pathway, *Eur. J. Med. Chem.* 86 (2014) 1–11.
- [51] K.K. Singh, Mitochondria damage checkpoint in apoptosis and genome stability, *FEMS Yeast Res.* 5 (2004) 127–132.
- [52] R. Wang, Y.-Y. Liu, X.-Y. Liu, S.-W. Jia, J. Zhao, D. Cui, L. Wang, Resveratrol protects neurons and the myocardium by reducing oxidative stress and ameliorating mitochondria damage in a cerebral ischemia rat model, *Cell. Physiol. Biochem.* 34 (2014) 854–864.
- [53] K.K. Singh, Mitochondria damage checkpoint, aging, and cancer, *Ann. NY Acad.*

Sci. 1067 (2006) 182–190.

[54] J.H. Santos, J.N. Meyer, B. Van Houten, Mitochondrial localization of telomerase as a determinant for hydrogen peroxide-induced mitochondrial DNA damage and apoptosis, *Hum. Mol. Genet.* 15 (2006) 1757–1768.

[55] J.H. Santos, J.N. Meyer, M. Skorvaga, L.A. Annab, B. Van Houten, Mitochondrial hTERT exacerbates free-radical-mediated mtDNA damage, *Aging cell* 3 (2004) 399–411.

[56] J.F. Passos, G. Saretzki, T. von Zglinicki, DNA damage in telomeres and mitochondria during cellular senescence: is there a connection?, *Nucleic Acids Res.* 35 (2007) 7505–7513.

[57] S.Y. Park, B. Choi, H. Cheon, Y.K. Pak, M. Kulawiec, K.K. Singh, M.-S. Lee, Cellular aging of mitochondrial DNA-depleted cells, *Biochem. Bioph. Res. Commun.* 325 (2004) 1399–1405.

[58] H. Kimura, K. Shintani-Ishida, M. Nakajima, S. Liu, K. Matsumoto, K.-I. Yoshida, Ischemic preconditioning or p38 MAP kinase inhibition attenuates myocardial TNF  $\alpha$  production and mitochondria damage in brief myocardial ischemia, *Life Sci.* 78 (2006) 1901–1910.

[59] A. Fradet-Turcotte, M.D. Canny, C. Escribano-Díaz, A. Orthwein, C.C.Y. Leung, H. Huang, M.-C. Landry, J. Kitevski-LeBlanc, S.M. Noordermeer, F. Sicheri, D. Durocher, 53BP1 is a reader of the DNA-damage-induced H2A Lys 15 ubiquitin mark, *Nature* 499 (2013) 50–54.

[60] B. Chakravarti, M. Ranjani, J.A. Siddiqui, B. Hemant Kumar, S.M. Rajendran, Prem P. Yadav, K. Rituraj, In vitro anti-breast cancer activity of ethanolic extract of *Wrightia tomentosa*: role of pro-apoptotic effects of oleanolic acid and urosolic acid, *J. Ethnopharm.* 142 (2012) 72–79.

- [61] A. De Cian, G. Cristofari, P. Reichenbach, E. De Lemos, D. Monchaud, M.-P. Teulade-Fichou, K. Shin-ya, L. Lacroix, J. Lingner, J.-L. Mergny, Reevaluation of telomerase inhibition by quadruplex ligands and their mechanisms of action, *PNAS* 104 (2007) 17347–17352.
- [62] J.E. Reed, A.A. Arnal, S. Neidle, R. Vilar, Stabilization of G-quadruplex DNA and inhibition of telomerase activity by square-planar nickel(II) complexes, *J. Am. Chem. Soc.* 128 (2006) 5592–5993.
- [63] S.-T. Von, H.-L. Seng, H.-B. Lee, S.-W. Ng, Y. Kitamura, M. Chikira, C.-H. Ng, DNA molecular recognition and cellular selectivity of anticancer metal(II) complexes of ethylenediaminediacetate and phenanthroline: multiple targets, *J. Biol. Inorg. Chem.* 17 (2012) 57–69.
- [64] L. Xu, X. Chen, J. Wu, J. Wang, L. Ji, H. Chao, Dinuclear ruthenium(II) complexes that induce and stabilise G-quadruplex DNA, *Chem. Eur. J.* 21 (2015) 4008–4020.

### Figure legends

**Fig. 1.** ORTEP drawing of complex **1**. Thermal ellipsoids for non-hydrogen atoms are drawn at a level of 30% probability.

**Fig. 2.** ORTEP drawing of complex **2**.

**Fig. 3.** ORTEP drawing of complex **3**.

**Fig. 4.** Ir or Pt contents in the Hep-G2 cancer cells (A) and different cellular fractions (B). ICP-MS was used to determine the metal contents.

**Fig. 5.** RT-PCR analysis of the expression level of c-myc and hTERT in the Hep-G2

cells treated with complexes **1–3** at their IC<sub>50</sub> concentrations for 24 h.

**Fig. 6.** Western blot analysis of the expression level of c-myc and hTERT in the Hep-G2 cells treated with complexes **1–3** at their IC<sub>50</sub> concentrations for 24 h. (A) C-myc and hTERT protein levels in Hep-G2 cells were analyzed by western blot. (B) The whole-cell extracts were prepared and analyzed by Western blot analysis using antibodies against c-myc and hTERT. The same blots were stripped and re-probed with a  $\beta$ -actin antibody to show equal protein loading. Western blot bands from three independent measurements were quantified with Image J. in (B), with the mean  $\pm$  SD (standard error of the mean).

**Fig. 7.** Inhibition of the telomerase activity by complexes **1–3** at their IC<sub>50</sub> concentrations in the Hep-G2 cancer cells for 24 h.

**Fig. 8.** Transfection of the EGFP plasmid (A) and the c-myc plasmid (B) in the Hep-G2 tumor cells. In (A), the cells were imaged using a Nikon Te2000 microscope (magnification 200 $\times$ ). In (B), the transfected cells were treated complexes **1–3** at their IC<sub>50</sub> concentrations for 24 h. The expression level of c-myc was determined by a multi-model plate reader with luciferase reporter gene assay kit.

**Fig. 9.** Fluorescence spectroscopic characterization of the Hep-G2 cells treated with complexes **1–3** at their IC<sub>50</sub> concentrations for 24 h. The treated cells were stained by the JC-1 dye and imaged using a Nikon Te2000 microscope (magnification 200 $\times$ ).

**Fig. 10.** Determination of ROS generation in the Hep-G2 cells treated with complexes **1–3** at their IC<sub>50</sub> concentrations for 24 h. The treated cells were stained by an oxidant-sensitive fluorescent probe, 2',7'-dichlorofluoresceindiacetate (DCFDA) and imaged using a Nikon Te2000 microscope (magnification 200 $\times$ ).

**Fig. 11.** Western blot analysis of the effects of complexes **1–3** on the expression levels of proteins involved in mitochondrion-initiated apoptosis. (A) The apoptosis related

proteins protein levels in Hep-G2 cells were analyzed by western blot. (B) The whole-cell extracts were prepared and analyzed by Western blot analysis using antibodies against apoptosis related proteins. The same blots were stripped and re-probed with a  $\beta$ -actin antibody to show equal protein loading. Western blot bands from three independent measurements were quantified with Image J. in (B).

**Fig. 12.** Flow cytometry analysis of the effects of complexes **1–3** on the levels of active caspase-3 and caspase-9 in the Hep-G2 cells.

**Fig. 13.** Apoptosis rate of the Hep-G2 cells. These Hep-G2 cells were the three Ir complexes **1–3** at their  $IC_{50}$  concentrations for 24 h and stained with Annexin V-FITC and PI, followed by flow cytometry analysis.

**Scheme 1.** Synthetic routes for three terpyridine ligands and the corresponding Ir complex **1–3**.

**Table 1.**  $IC_{50}^a$  values ( $\mu M$ ) of 3-MeO-Phtpy, 2-MeO-Phtpy, 4-MeO-Phtpy, cisplatin, and complexes **1–3** on the five selected human cell lines.

Compound	BEL-7404	Hep-G2	NCI-H460	MGC80-3	HL-7702 <sup>c</sup>
3-MeO-Phtpy	34.34 $\pm$ 1.02	19.67 $\pm$ 0.73	19.96 $\pm$ 0.35	20.96 $\pm$ 0.31	35.11 $\pm$ 0.81 (1.78)
<b>1</b>	27.77 $\pm$ 0.59	3.19 $\pm$ 1.15	6.93 $\pm$ 0.44	8.68 $\pm$ 1.05	37.51 $\pm$ 0.56 (11.76)
2-MeO-Phtpy	36.94 $\pm$ 0.80	26.40 $\pm$ 1.45	24.73 $\pm$ 1.10	23.02 $\pm$ 1.44	17.16 $\pm$ 1.03 (0.65)
<b>2</b>	31.29 $\pm$ 1.30	6.63 $\pm$ 1.01	10.42 $\pm$ 1.39	14.69 $\pm$ 2.12	31.46 $\pm$ 1.69 (4.75)
4-MeO-Phtpy	56.78 $\pm$ 0.65	28.43 $\pm$ 0.39	33.78 $\pm$ 1.76	35.71 $\pm$ 0.92	18.11 $\pm$ 1.07 (0.64)
<b>3</b>	38.27 $\pm$ 0.43	15.08 $\pm$ 0.62	27.91 $\pm$ 0.93	22.09 $\pm$ 0.71	39.13 $\pm$ 0.53 (2.59)
Cisplatin <sup>b</sup>	16.91 $\pm$ 1.01	18.68 $\pm$ 0.67	18.01 $\pm$ 1.23	13.99 $\pm$ 0.76	17.98 $\pm$ 1.94 (0.96)

<sup>a</sup>The  $IC_{50}$  values are presented as mean $\pm$ SD (standard error of the mean) from five or six independent experiments. <sup>b</sup> Cisplatin was prepared at a concentration of 1.0 mM in

a 0.154 M NaCl solution [34,35]. <sup>c</sup> The selectivity index factors, defined as  $IC_{50}$  (HL-7702 cells)/ $IC_{50}$  (Hep-G2 tumor cells), are shown in parentheses.[36,37]

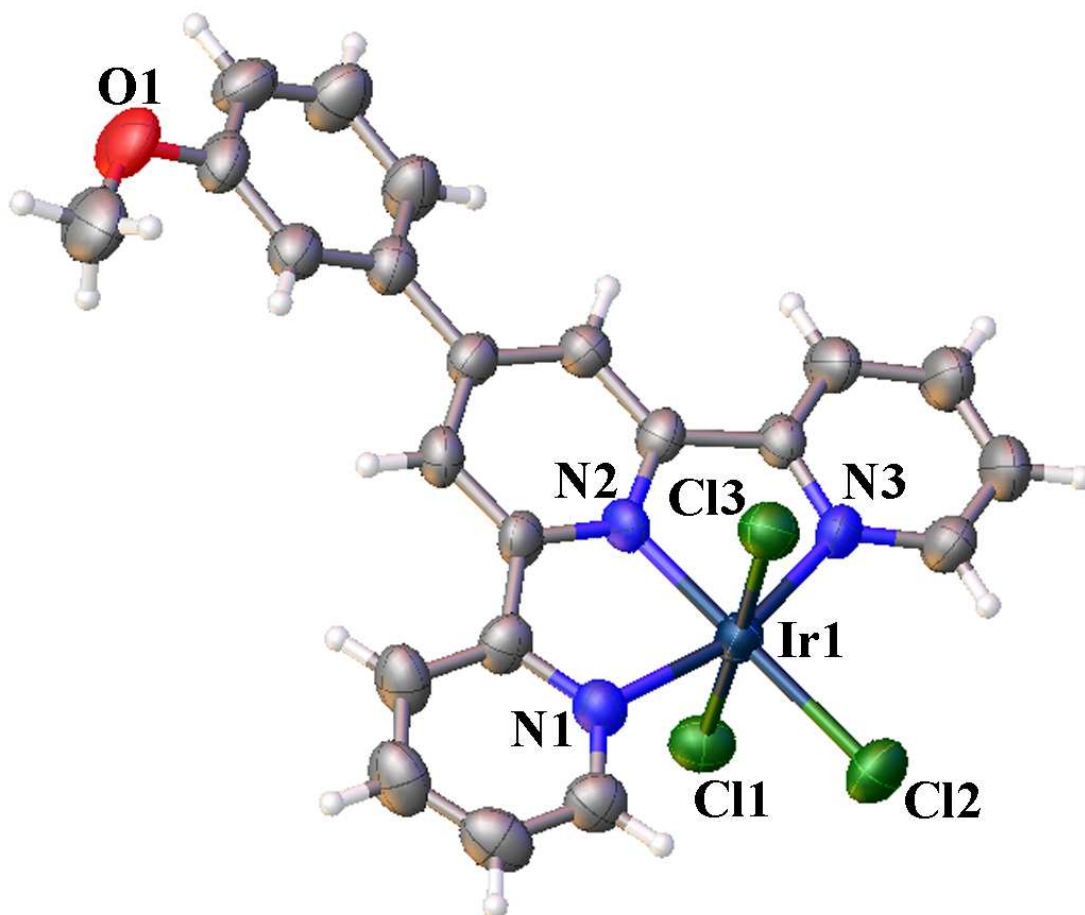


Fig. 1

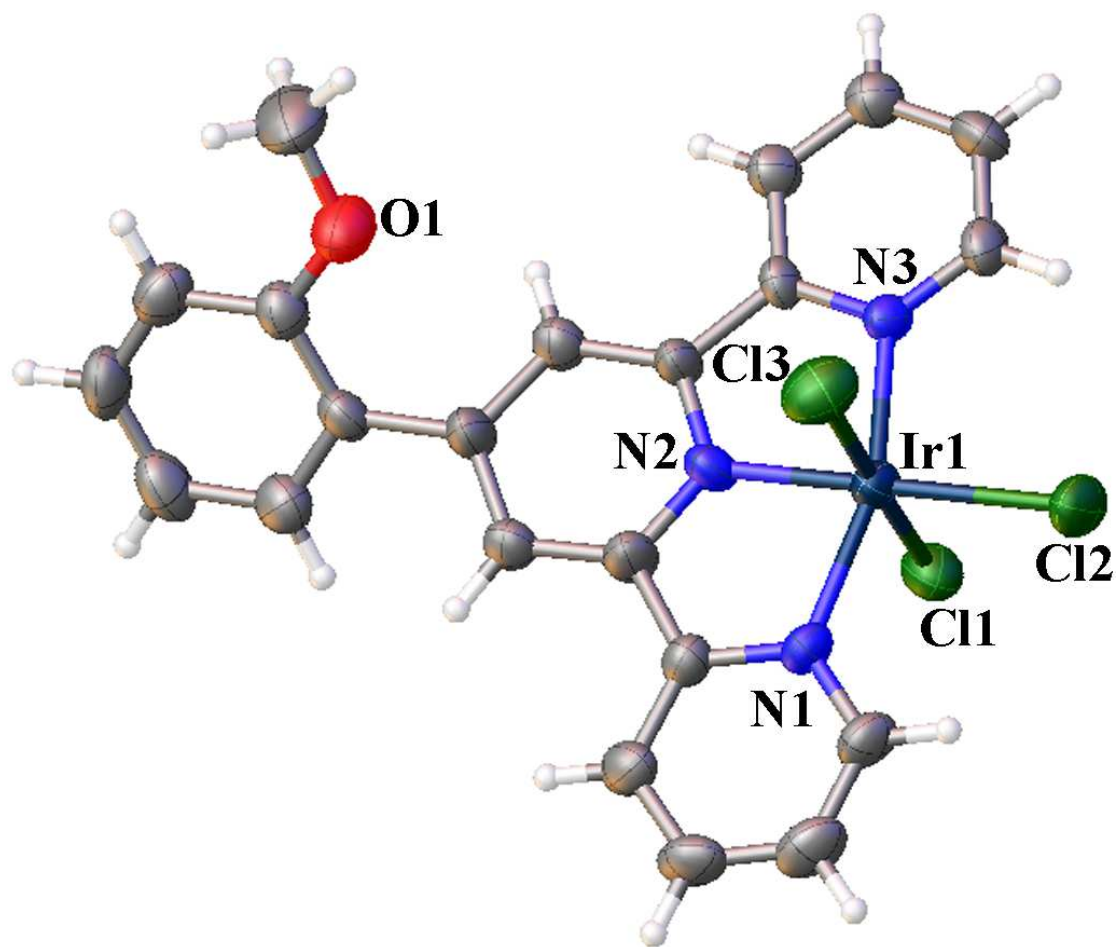


Fig. 2

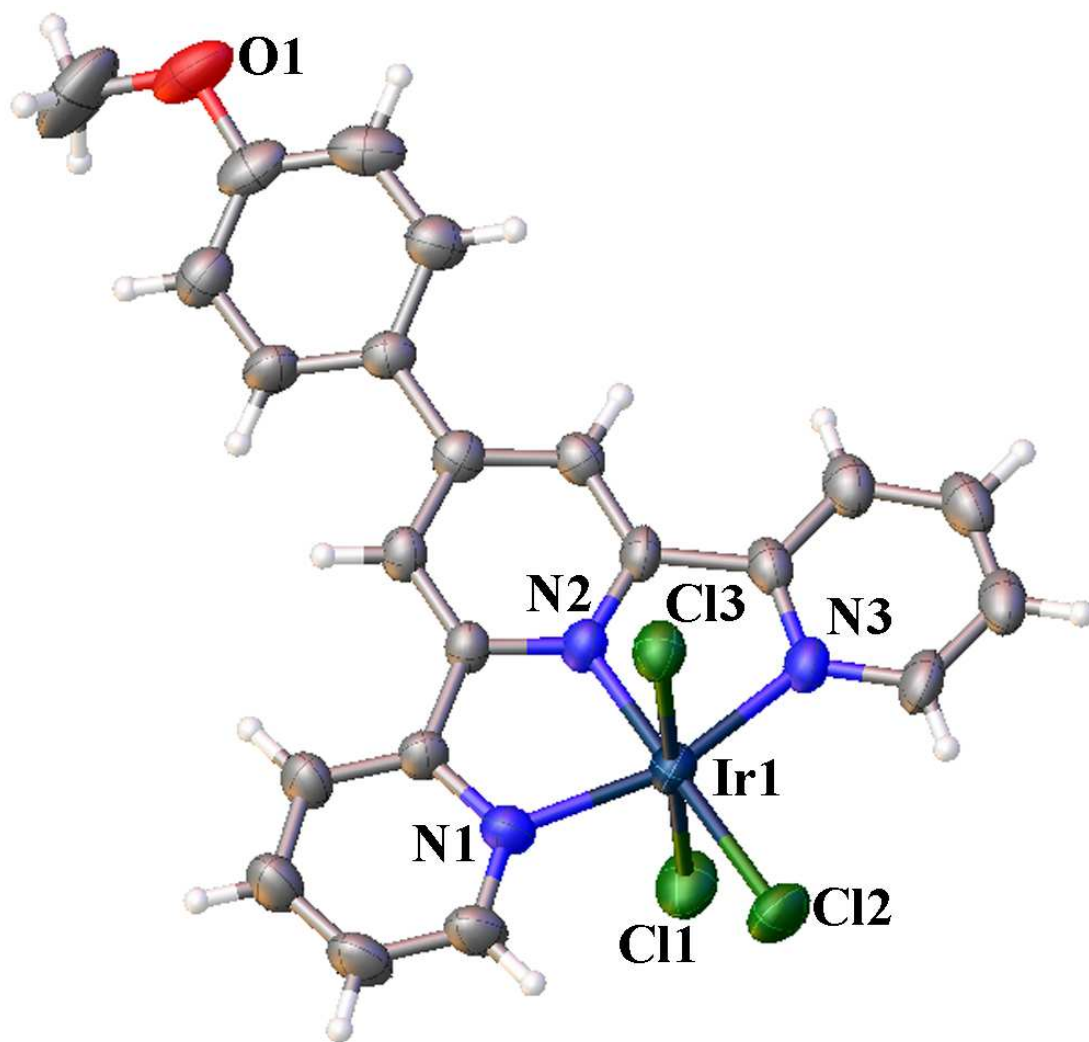


Fig. 3

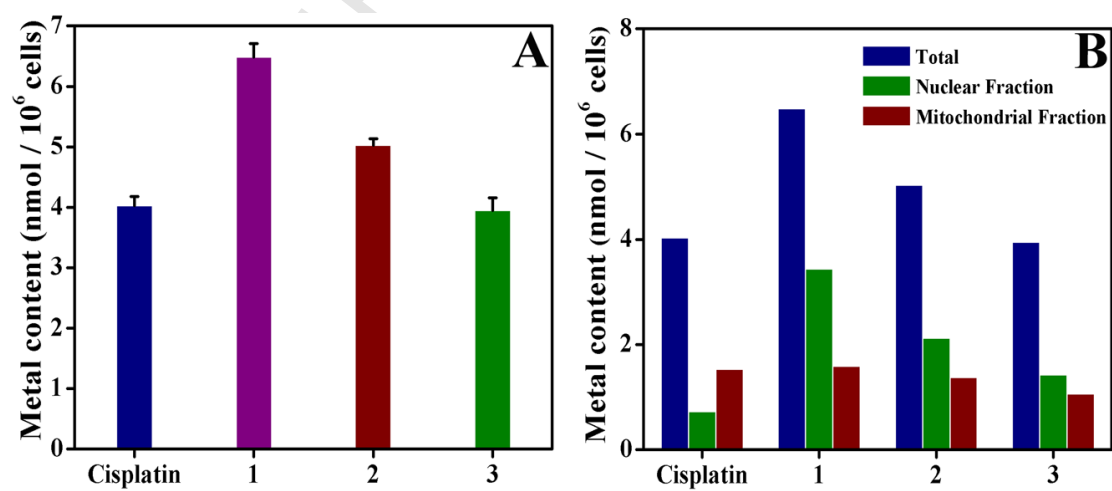


Fig. 4

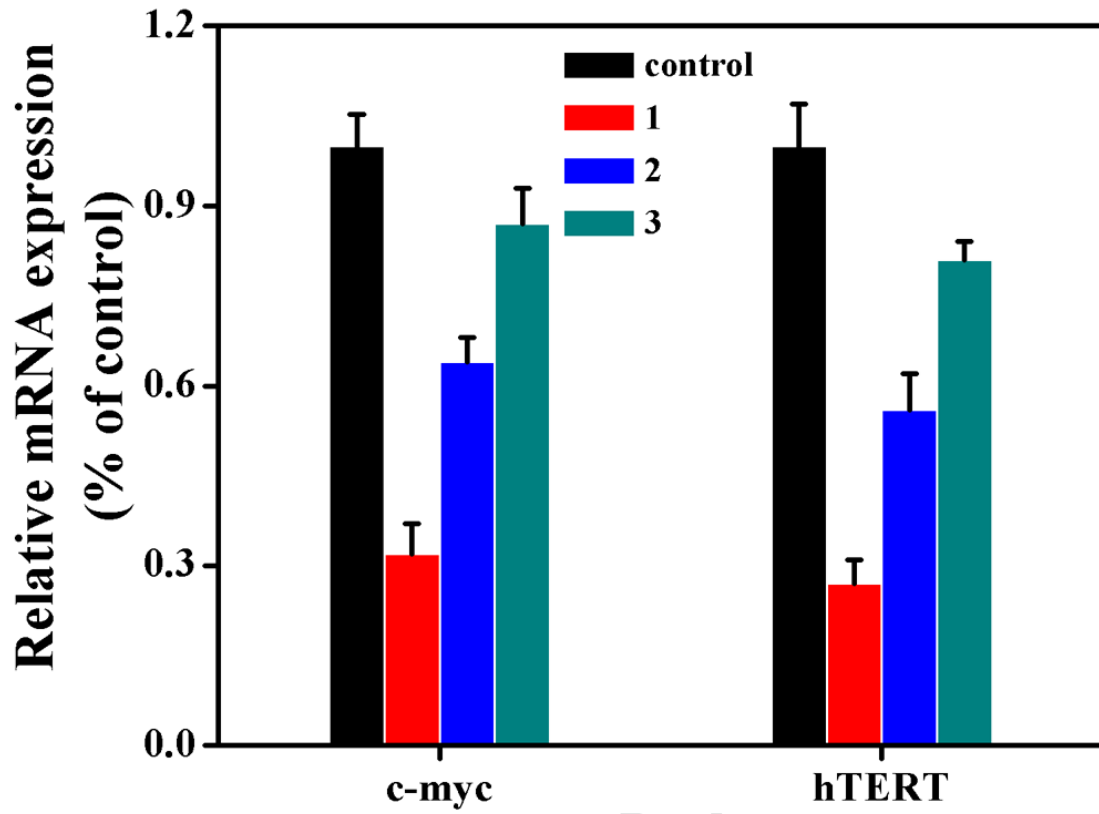


Fig. 5

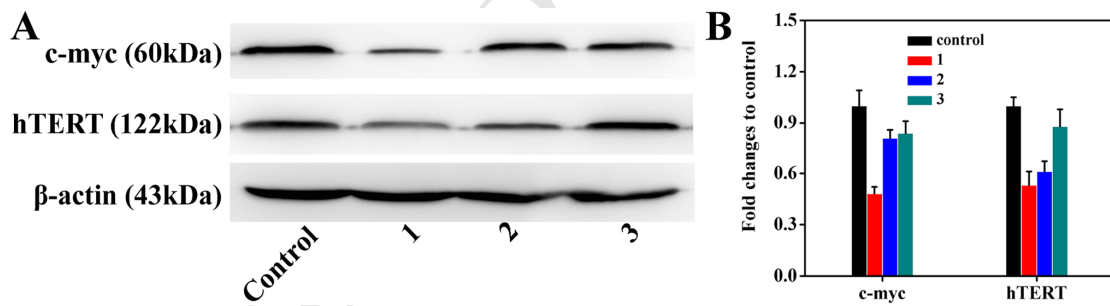


Fig. 6



Fig. 7

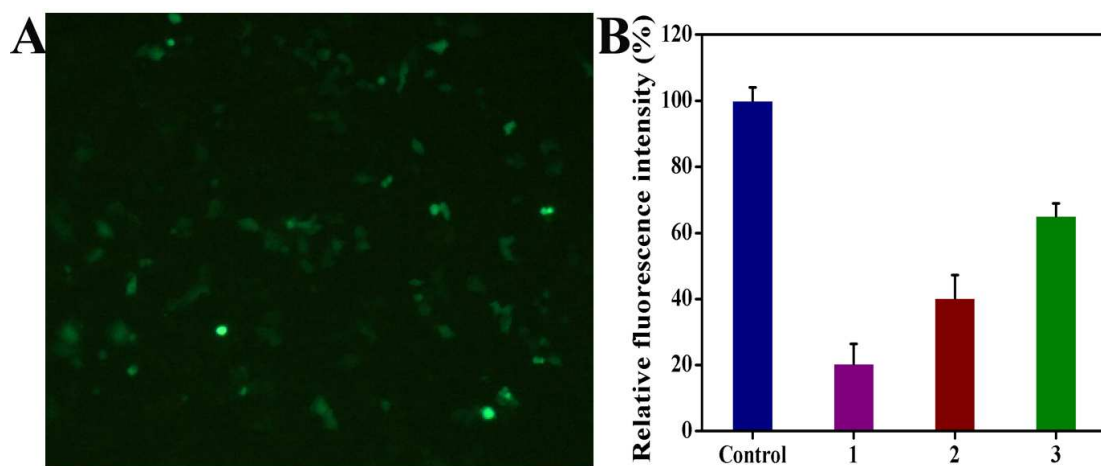


Fig. 8

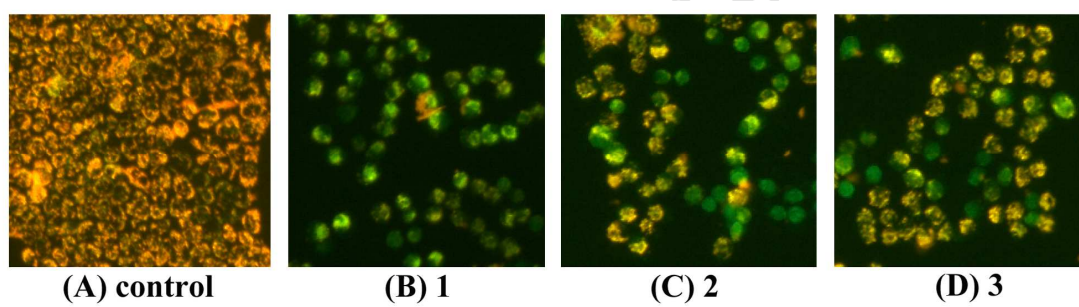


Fig. 9

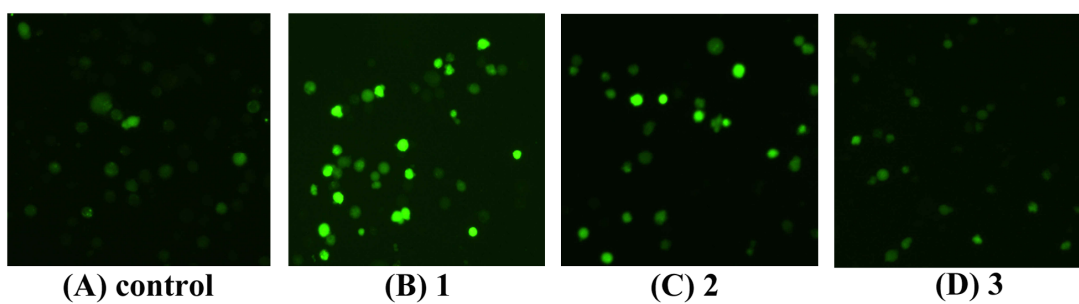


Fig. 10

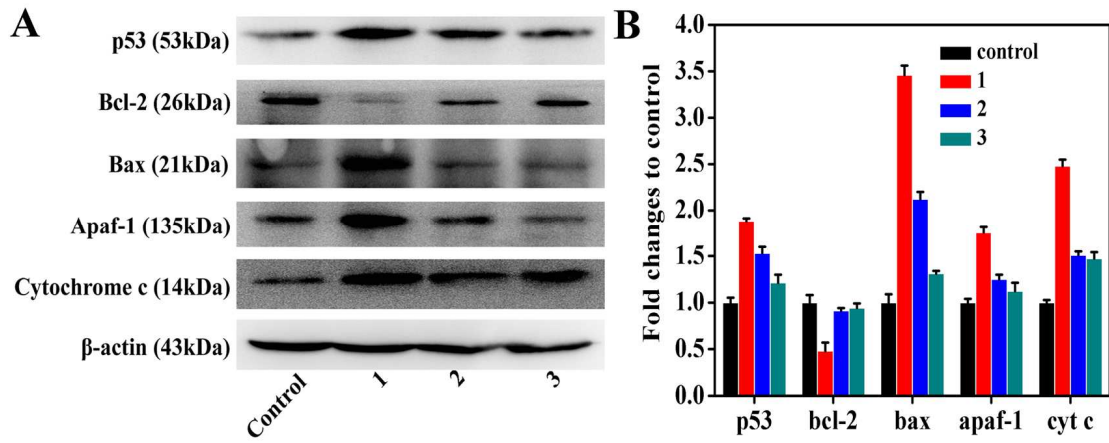


Fig. 11

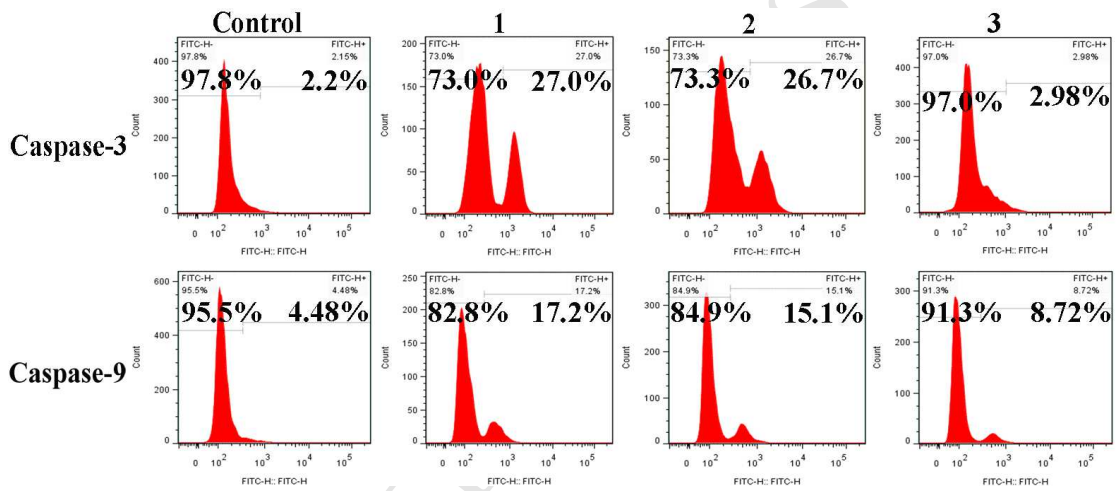


Fig. 12

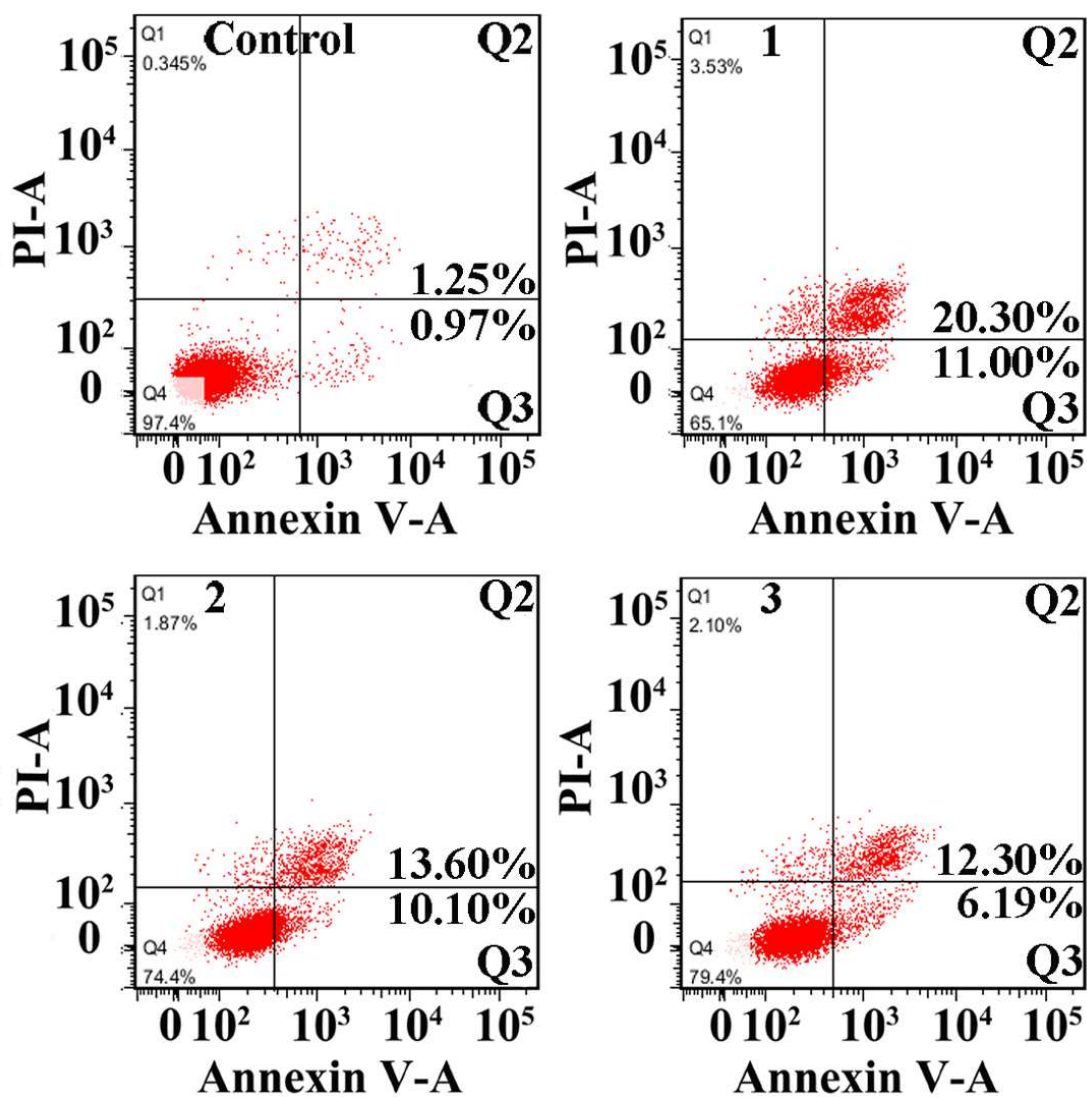
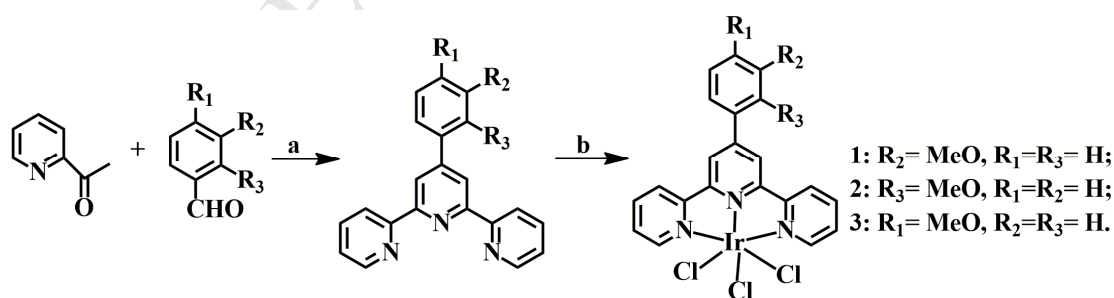


Fig. 13



Scheme 1

**Highlights:**

- There iridium(III) complexes with terpyridine ligands were synthesized and characterized.
- Complexes **1–3** directly targeted c-myc promoter elements and inhibited the telomerase activity
- **1–3** may trigger cell apoptosis via a mitochondrial dysfunction pathway